Stability of input voltages of a three-level inverter NPC fed by photovoltaic sources

F. Bouchafaa [1*] , A. Chouder [2] and S. Boukhalfa [1†]

[1] Laboratory of Instrumentation, Faculty of Electronics and Computer
University of Sciences and Technology Houari Boumediene, 'USTHB'
PO Box 32, El-Alia, Bab-Ezzouar, Algiers, Algeria

[2] Photovoltaic Solar Energy Division, Centre for Development of Renewable Energy, 'CDER'
PO Box 62, Road Observatory, Bouzareah, Algiers, Algeria

(reçu le 15 Mai 2012 - accepté le 30 Octobre 2012)

Abstracts - *In this paper we study the stability of input voltages of the cascade consisting of a photovoltaic inverter and a three-level structure NPC, feeding a synchronous machine with permanent magnets (PMSM) commissioned by the speed command flow oriented. For this, we first present the modeling of the Photovoltaic, then modeling and strategy to control the inverter three-level structure NPC. In the end, to address the mid-point fluctuation and instability of input voltages at the terminals of the inverter, proposed a solution consisting of a bridge clamping which gave promising results.*

Résumé - *Dans cet article, nous étudions la stabilité des tensions d'entrée de la chaîne composée d'un onduleur photovoltaïque et un onduleur à trois niveaux à structure NPC, alimentant une machine synchrone à aimants permanents (MSAP) commandée en vitesse par le flux orienté. Pour cela, nous présentons d'abord la modélisation de générateur photovoltaïque, puis la modélisation et la stratégie de commande de variateur de fréquence à structure NPC. A la fin, pour répondre aux fluctuations de point milieu et l'instabilité des tensions d'entrée aux bornes de l'onduleur, les auteurs ont proposés une solution consiste à introduire un pont d'équilibrage des tensions à base d'un hacheur série en parallèle de chaque condensateurs qui a donné des résultats prometteurs.*

Keywords: Photovoltaic generator - Multilevel PWM inverter - Digital MPPT - Voltage stability - Clamping bridge - PMSM.

1. INTRODUCTION

The growth of energy demand in the world stimulated the search for new sources of energy, and solar energy is one of the most unconventional promising.

In this concept, photovoltaic systems offer the possibility of converting sunlight into electricity. The transformation of electricity through the photovoltaic effect can provide energy services and to meet many needs in its flexibility and ease of installation and maintenance.

In the present work focuses on the use of solar energy which is great. Natural source of energy and free, whose applications are very diverse. The use of renewable energy is growing significantly in the world. Algeria, a country whose geographical location is ideal to make the most of solar energy, especially the desert regions.

* fbouchafa@gmail.com, aissachouder@gmail.com
† saidaboukhalfa@yahoo.fr

Feeding by a sinusoidal voltage source plays a role in the industrial field. The last decade has been marked by unprecedented technological advances in the field of power electronics.

On the one hand, the power switches used in the structures of converters are able to switch more quickly, On the other hand, new structures have emerged converters. Some of them promote high switching frequencies. And instead to transfer significant levels of power (multi-level structures,.).

As part of our work, we will focus on voltage inverter at three levels to NPC structure. The latter can increase the voltage supplied to the load through their topology. Thus, they can generate more voltage sinusoidal possible and improve the total harmonic distortion through the high voltage levels provided by the structure of this new converter.

2. ELECTRICAL MODEL OF PHOTOVOLTAIC CELL

To find the model of the photovoltaic generator, we must first find the electrical equivalent to that source. Many mathematical models have been developed to represent their highly nonlinear resulting from that of semiconductor junctions that are the basis of their achievements.

Found in the literature several models of different photovoltaic generators them through the procedure and the number of parameters involved in the calculation of voltage and current end-of photovoltaic generator. We will present our work in the model with two diodes; in fact this model takes into account the different internal resistance of the PV cell, (Fig. 1) [1].

It consists of a current source i_{ph} that models the conversion of light energy flow electrical resistance R_p shunt is a consequence of leaks by the side effect on the photovoltaic cell, a series resistance R_s, representing the various resistance contact and connection and two diodes D_1 and D_2 in parallel model the PN junction [2].

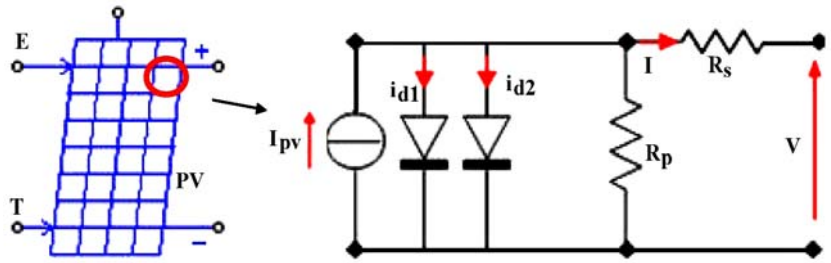

Fig. 1: Model of a photovoltaic cell with two diodes

The current generated by the module is given by the following equation

$$\begin{cases} I = I_{ph} - I_{d1} - I_{d2} - I_{RP} \\ I = I_{ph} - I_{S1}\times\left(\exp\frac{q\times(V+R_s\times I)}{A_1\times K\times T}-1\right) - I_{S2}\times\left(\exp\frac{q\times(V+R_s\times I)}{A_2\times K\times T}-1\right) - \frac{V+R_s\times I}{R_p} \end{cases} \quad (1)$$

with, I, Current delivered by the module. I_{d1}, I_{d2}, Fluent in both diodes D_1 and D_2, I_{RP}, Current in resistance R_P, I_{ph}, Photo-current, I_{S1}, I_{S2}, Current saturation of the two diodes, A_1, A_2, Ideality factor of the junction of D_1 and D_2, q, Charge of the electron, K, Constant Boltzman, T, Temperature junction, R_S, Resistance series, R_p, Resistance shunt.

Thus the electrical diagram equivalent of 'GPV' into a block diagram (Fig. 2) with four variables.

- The two input variables are the sunshine (E_S) and the temperature junction cells (T_j);
- The output variables are the current supplied by the 'GPV' (I) and the terminal voltage of 'GPV' (V).

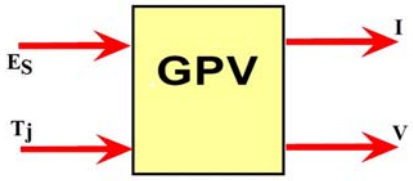

Fig. 2: Block diagram of a photocell

The characteristics of a PV cell of changes in current and power based on the voltage of the PV cell is shown in figure 3.

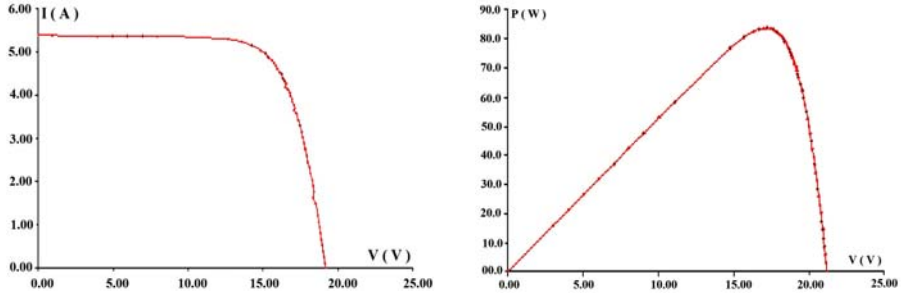

Fig. 3: Characteristics $I = f(V)$ and $P = f(V)$
of a MSX-83, T = 25 °C and E = 1000 W/m^2

3. STRUCTURE OF THE THREE-PHASE INVERTER THREE LEVELS

Many multilevel converter topologies have been devised and implemented. We will present the converter clamped by the neutral (NPC).

The inverter voltage phase three-level NPC structure presented in figure 4, consists of twelve two-way switches and six unidirectional switches connected to the midpoint of the two sources allowing access to potential $-U_{c/2}, 0, +U_{c/2}$.

Each arm is equivalent to a three-position switch to get out at three levels of voltage $+U_{c1}, 0, -U_{c2}$, [3].

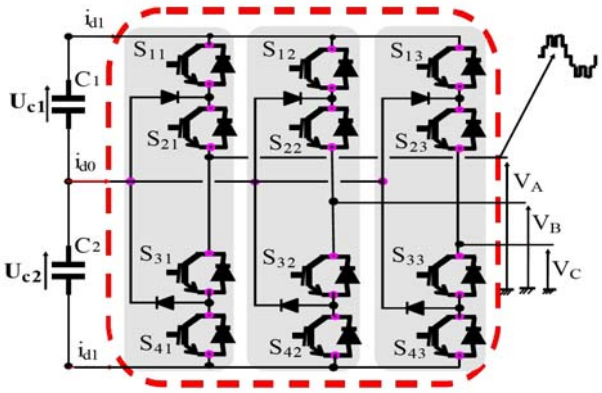

Fig. 4: Topology of the inverter three phases three-level

3.1 Knowledge and control model of a three-level NPC VSI

In order to deduce the knowledge model of the inverter, we introduce the connection function S_{is} of the switch which describes the state of every switch (1 = closed, 0 = opened). In this function ' i ', is the number of the of the commutation cell, $i \in \{1,2,3\}$, s , is the number of the semi-conductor.

The output voltages of the inverter relatively to the middle point M with using the connection functions of the half-arm (S_{i1}^b, S_{i0}^b) are defined as follows:

$$\begin{bmatrix} V_A \\ V_B \\ V_C \end{bmatrix} = \frac{1}{3}\begin{bmatrix} 2 & -1 & -1 \\ -1 & 2 & -1 \\ -1 & -1 & 2 \end{bmatrix} \times \left\{ \begin{bmatrix} S_{11}^b \\ S_{21}^b \\ S_{31}^b \end{bmatrix} \times U_{C1} - \begin{bmatrix} S_{10}^b \\ S_{20}^b \\ S_{30}^b \end{bmatrix} \times U_{C2} \right\} \tag{2}$$

with, $S_{i1}^b = S_{i1} \times S_{i2}$, $S_{i0}^b = S_{i3} \times S_{i4}$

The input currents of the inverter are given as follow:

$$\begin{cases} i_{d1} = S_{11}^b \times i_1 + S_{21}^b \times i_2 + S_{31}^b \times i_3 \\ i_{d2} = S_{10}^b \times i_1 + S_{20}^b \times i_2 + S_{30}^b \times i_3 \\ i_{d0} = \left(1 - S_{11}^b - S_{10}^b\right) \times i_1 + \left(1 - S_{21}^b - S_{20}^b\right) \times i_2 + \left(1 - S_{31}^b - S_{30}^b\right) \times i_3 \end{cases} \tag{3}$$

In order to develop a control model of this inverter, we define the average model of the knowledge one. Thus, we define the generating function ' X_g ' of a discontinuous one ' X ', as the mean value of ' X ' on a modulation period ' T_e ' supposed very small [3, 4]. The real time evolution of the modulated voltage may be approximated by the equivalent mean value during the modulation period (T_e):

$$\left\langle u_g(t)\right\rangle = \left[\frac{1}{T_e}\times\int_{kT_e}^{(k+1)T_e} u(t)\times dt\right]_{T_e\to 0}, \quad k\in N \tag{4}$$

The control model of the three phases three-level NPC VSI, deduced from the system (2), is given by the following equation where $\langle V_A\rangle$, $\langle V_B\rangle$ and $\langle V_C\rangle$ represent the mean value of the instantaneous ones.

$$\begin{bmatrix}\langle V_A\rangle\\ \langle V_B\rangle\\ \langle V_C\rangle\end{bmatrix} = \frac{1}{3}\begin{bmatrix}2 & -1 & -1\\ -1 & 2 & -1\\ -1 & -1 & 2\end{bmatrix}\times\left\{\begin{bmatrix}(S_{11}^b)_g\\ (S_{21}^b)_g\\ (S_{31}^b)_g\end{bmatrix}\times U_{C1} - \begin{bmatrix}(S_{10}^b)_g\\ (S_{20}^b)_g\\ (S_{30}^b)_g\end{bmatrix}\times U_{C2}\right\} \tag{5}$$

3.2 New calculated PWM strategy of the three-level inverter

For the NPC inverter, most carrier based PWM schemes that have been investigated derive from the carrier disposition strategies originally proposed by Carrara *et al.* [3]. In this part, we present a digital strategy which uses the control model of the three-level voltage inverters.

For the three-level inverter, two identical saw tooth carriers (Fig. 5) U_{m1} and U_{m2} (of frequency f_m) with of a phase shift of ($1/2\,f_m$) between them are used to improve the total harmonic distortion.

The different steps of the algorithm digital strategy are expressed by:

Step1: Compute of the generating conversion simple functions n_{gi}

$$n_{gi} = V_{refi} \,/\, U_c \tag{6}$$

with, $i\in\{1, 2, 3\}$, V_{redi}, Reference voltage of the phase i.

Step 2: Computation of the half arm connection generating functions S_{ing}^b, (Fig. 6)

$$S_{i1g}^g = \frac{n_{gi}}{2} \text{ and } S_{i0g}^g = -\frac{n_{gi}}{2} \tag{7}$$

n_{gi}, S_{ing}^b are respectively the generator conversion and half arm connection functions.

Step 3: Computation of the half arm connection functions S_{ing}^b

We define two instants T_{i1}, T_{i0}

$$\begin{cases} T_{i1} = T_h\times\left\{1-\left|S_{i1g}^b\right|\right\}\\ T_{i0} = T_h\times\left\{1-\left|S_{i0g}^b\right|\right\}\end{cases} \tag{8}$$

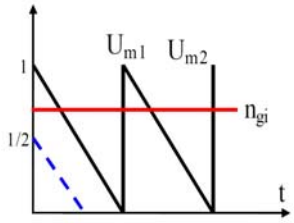

Fig. 5: Saw tooth carriers

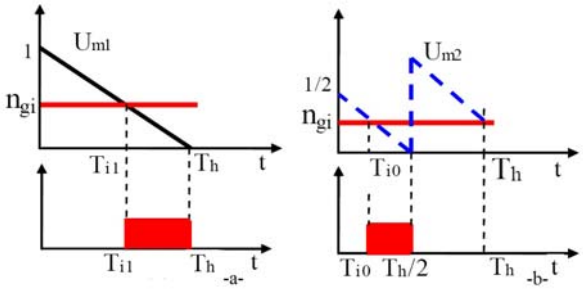

Fig. 6: Carriers U_{m1} and U_{m2}

$$\begin{cases} \left(T_{i0} \le t \le \dfrac{T_h}{2} \right) \text{ or } \left(T_{i1} \le t \le T_h \right) \Rightarrow a_i = 1 \\ \left(t < T_{i_0} \right) \text{ or } \left(\dfrac{T_h}{2} < t < T_{i1} \right) \Rightarrow a_i = 0 \end{cases} \tag{9}$$

$$\begin{cases} \left(S^b_{i\,lg} > 0 \right) \Rightarrow \left(S^b_{il} = a_i \right) \text{ and } \left(S^b_{i0} = 0 \right) \\ \left(S^b_{i\,lg} \le 0 \right) \Rightarrow \left(S^b_{il} = 0 \right) \text{ and } \left(S^b_{i0} = a_i \right) \end{cases}$$

In this algorithm, the variable t is reinitialized at the each end of the period T_h.

The next step is using to find the connection functions S_{is} from the instantaneous functions:

$$\begin{cases} \left(\left(S^b_{il} = 1 \right) \text{ and } \left(S^b_{i0} = 1 \right) \right) \text{ or } \left(S_{il} = 1 \right) \text{ and } \left(S_{i2} = 0 \right) \\ \quad \Rightarrow \left(S_{il} = 1 \right) \text{ and } \left(S_{i2} = 0 \right) \\ \left(S^b_{il} = 1 \right) \text{ and } \left(S^b_{i0} = 0 \right) \Rightarrow \left(S_{il} = 1 \right) \text{ and } \left(S_{i2} = 0 \right) \\ \left(S^b_{il} = 0 \right) \text{ and } \left(S^b_{i0} = 1 \right) \Rightarrow \left(S_{il} = 0 \right) \text{ and } \left(S_{i2} = 0 \right) \end{cases} \tag{10}$$

Then the command of the inverter's switches is obtained as expressed by:

$$\begin{cases} S_{is} = 1 \Leftrightarrow B_{is} = 1 \quad (\text{switch is closed}) \\ S_{is} = 0 \Leftrightarrow B_{is} = 0 \quad (\text{switch is open}) \end{cases} \tag{11}$$

3.3 Simulation result

The result of the simulation for the modulation index $m = 12$ and 27 (m is the ratio of carrier frequency to the reference signal frequency) and $r = 0.8$ (r is the ratio of the reference signal magnitude to the carrier amplitude) are shown in figure 7.

Figure 7 represents the simple output voltage of the three-level NPC VSI controlled by the proposed digital strategy with two bipolar carriers.

We notice that, for even values of m, the simple output voltage has symmetry relatively to the quarter of the period, and we have only odd harmonics. But for odd

values of m , we have no symmetry, and then even and odd harmonics exist (Fig. 7). The voltage harmonics gather by families centred around frequencies multiple of $2m_f$ (Fig. 7).

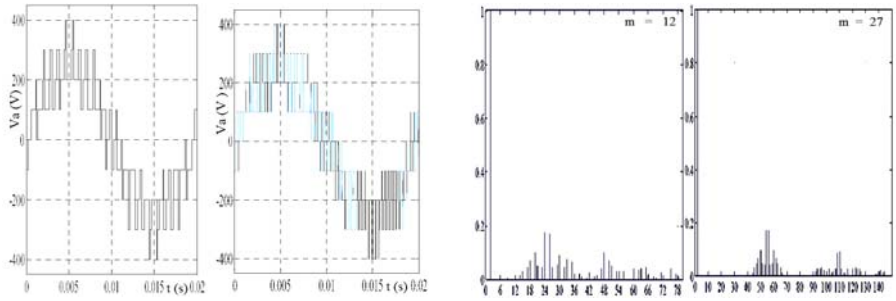

Fig. 7: The digital strategy of the three-level NPC VSI (simple and spectrum voltage)

The variation of the amplitude of the fundamental function of modulation rate ‘ r ’ is given in figure 8.

The modulation rate ‘ r ’ lets linear adjusting of the fundamental magnitude from $r = 0$ to $r_{max} = 1.2$ (Fig. 8). The total harmonics distortion (THD) decreases when r increases (Fig. 8).

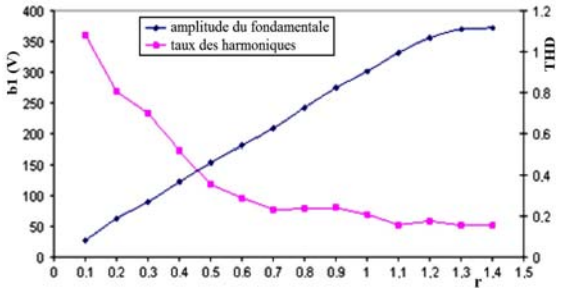

Fig. 8: Adjusting characteristic and the harmonics rate
of the output voltage of the inverter (m = 12)

4. PERMANENT MAGNET SYNCHRONOUS MACHINE DRIVE

The Well-established $d-q$ model of the wound rotor synchronous machine is easily adapted to study the performance of the permanent magnet synchronous motor (PMSM). The following assumptions are made in the derivation. The Park model of the permanent magnet synchronous machine, with p pairs of poles, is defined by the following equations system [5].

$$\begin{bmatrix} V_{ds} \\ V_{qs} \end{bmatrix} = \begin{bmatrix} R & -L_q\,\omega \\ L_d\,\omega & R \end{bmatrix} \times \begin{bmatrix} I_{ds} \\ I_{qs} \end{bmatrix} + \begin{bmatrix} L_d & 0 \\ 0 & L_q \end{bmatrix} \times \frac{d}{dt} \begin{bmatrix} I_{ds} \\ I_{qs} \end{bmatrix} + \omega \times \Phi_f \begin{bmatrix} 0 \\ 1 \end{bmatrix} \quad (12)$$

The electromagnetic torque is given by the following expression.

$$T_{em} = p\left[\Phi_d \times I_{qs} + \Phi_q \times I_{ds}\right] = p\left[(L_d - L_q) \times i_{ds} + \Phi_f\right] \times I_{qs} \qquad (13)$$

The control strategy often used consists to maintain the current i_{ds} to zero, and to control the speed by the current i_{qs} via the voltage V_{qs}. When the current i_{ds} is zero, the PMSM model presented in figure 9 is reduced, for the axis q, to separately excitation DC machine equivalent one. Regulate the current i_{ds} to zero lets have, for a given stator currents magnitude, a maximum torque. In this paper, we use the algorithm $i_{ds} = 0$ (Fig. 10) [5].

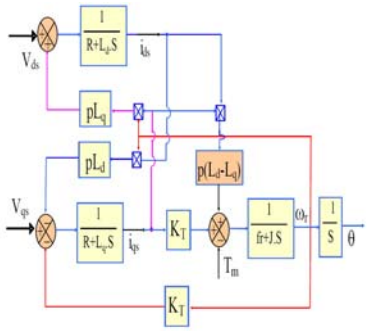

Fig. 9: The model of the PMSM

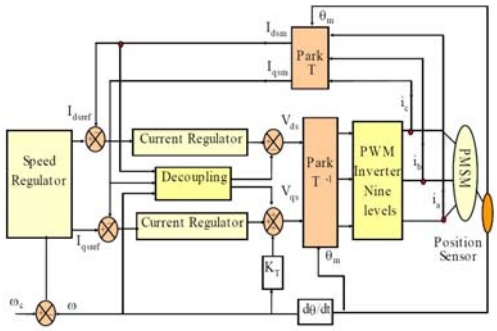

Fig. 10: The speed control using the algorithm

5. PHOTOVOLTAIC CELL-FILTER-THREE-LEVEL NPC VSI-CASCADE

Until now, we have supposed the input DC voltages of three-level NPC VSI constants. In this part, we study a generation input DC voltages manner. For this, we propose a cascade presented in the figure 11.

According to the intermediate filter, we can consider that the current i_{d1} and i_{d2} as perturbations, and current i_{pv} as a quantity of order. Thus, to control the output quantities U_{C1} and U_{C2}, it has only one magnitude adjustment i_{pv}.

Hence, we can deduce that it is practically impossible to have $U_{C1} = U_{C2}$ with a single source. So, for this type of cascade, the current i_{d0} is the source of the imbalance between the two input voltages U_{C1} and U_{C2} of the inverter at three levels, [6, 7].

The capacity of the intermediate filter has the same value ($C_1 = C_2 = 20$ mF).

We note the instability of input voltages U_{C1} and U_{C2} of the inverter shown in figure 12 to influence the behavior of the machine. By introducing a load torque between two instants, voltages U_{C1} and U_{C2} are increasing and the difference is not equal zero.

This fact accentuates the problem of unbalance of the different input DC voltages sources of three-level NPC VSI.

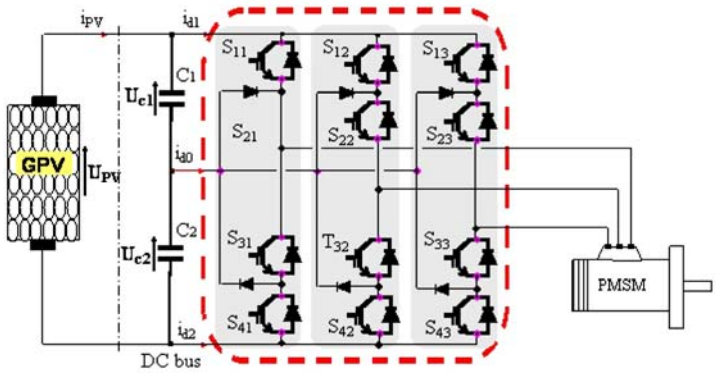

Fig. 11: Structure of the Cascade GSPV-Inverter three-level NPC-PMSM

Figure 13 shows the rate of supply voltage and the electromagnetic torque of PMSM for a reference speed. We note these variations of the output voltage of the inverter which increases the electromagnetic torque ripple, hence its influence on the performance of the machine.

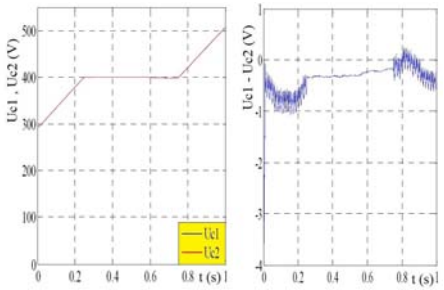

Fig. 12: The input DC voltages U_{C1}, U_{C2} and their differences

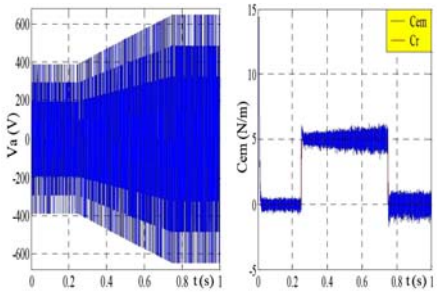

Fig. 13: Behavior of the conduct of the PMSM

5.1 Stabilization of input voltages of the inverter

To remedy to the problem of the instability of the output DC voltage of the photovoltaic cell, we propose to use a clamping bridge of the input DC voltages of multilevel inverter [8].

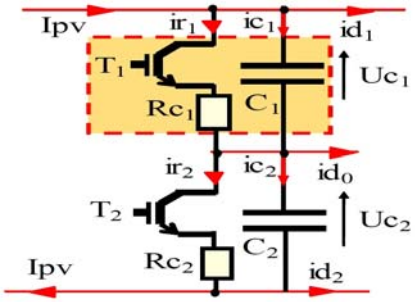

Fig. 14: The clamping bridge cell

The clamping bridge cell is a simple circuit constituted by a transistor and a resistor in series connected in parallel of capacitor as shown in figure 14. The transistors are controlled in order to maintain an equality of the different voltages.

In this part, the model of intermediate filter with clamping bridge is defined by following equation:

$$\begin{cases} C_1 \times \dfrac{dU_{c1}}{dt} = I_{pv} - i_{d1} - I_{r1} \\ C_2 \times \dfrac{dU_{c2}}{dt} = I_{pv} + i_{d2} - I_{r2} \end{cases} \tag{14}$$

In this part, the intermediate filter with clamping bridge is controlled by following algorithm:

$$\begin{cases} U_{ci} - U_{ref} = \varepsilon_i \\ \text{si} \quad \varepsilon_i > 0 \quad \text{on a :} \quad T_i = 1 \Rightarrow I_{ri} = T_i \times \dfrac{U_{ci}}{R_{ci}} \\ \text{si} \quad \varepsilon_i < 0 \quad \text{on a :} \quad T_i = 0 \Rightarrow I_{ri} = 0 \end{cases} \tag{16}$$

with, $i \in \{1, 2\}$.

5.2 Interpretation of results

The figures 15 and 16 show the simulation results to use the clamping bridge. We observe the input currents of the rectifier i_{d0} of three-level NPC VSI (Fig. 15). The currents i_{d1} i_{d1} is the opposite of the current i_{d2} i_{d2}. The current i_{d0} have a mean value practically null.

In the figures 16, we show the performances of the bridge clamping control of the output voltage of the photovoltaic cell. We note that, the output voltage is constant. Therefore the different input DC voltages of the three-level NPC VSI are constant and practically equal $U_{C1} = U_{C2}$.

The difference of the input voltages of three level NPC inverter is decrease to have a value practically null in steady states, and this difference is equal zero (Fig.16).

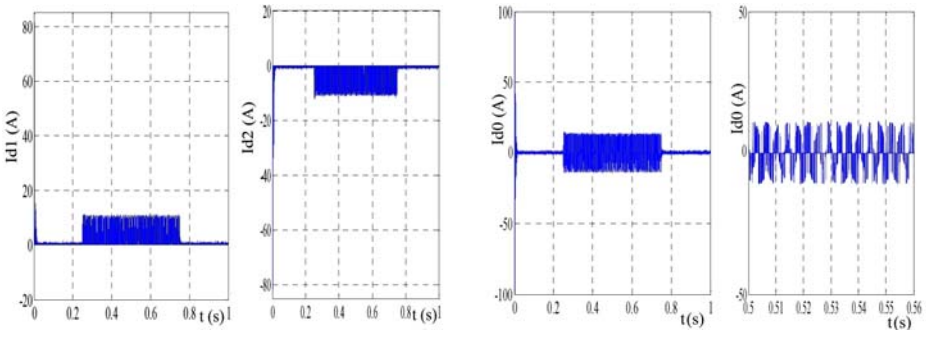

Fig. 15: The input current of the three-level inverter

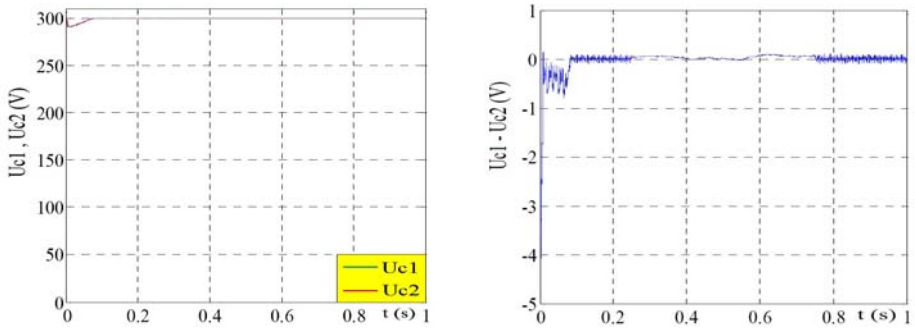

Fig. 16: The input DC voltages U_{C1}, U_{C2} and their differences

The performances of the speed control algorithm of the PMSM (Fig. 17). The PMSM is derived using vector control with direct current reference null.

The figure 17 shows the speed follows quietly its reference, the torque effect for the load variation, the output voltage of inverter and alimentation of machine are sinusoidal.

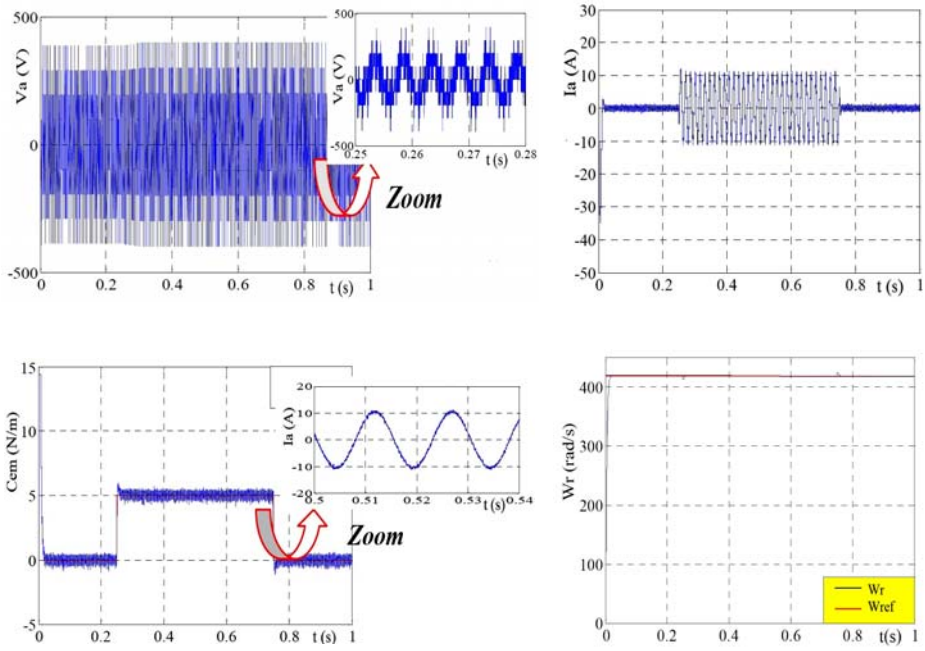

Fig. 17: The PMSM performances fed by three-level NPC inverter cascade

6. CONCLUSION

In this paper, we have studied stability problem of the input voltage of the three-level NPC inverter fed by photovoltaic cell.

The study of the stability problem of the input voltages of three-level NPC inverter using a cascade constituted by photovoltaic cell-filter-three-level NPC VSI.

The application of the clamping bridge shows parfait following of the input DC and his reference and the stability of the input voltage of three-level NPC inverter. have shows is possible to conceiver, with frequency charger using in output the three-level inverter, PMSM variator with feeble rate of harmonics.

The results obtained with this solution confirm the good performances of the proposed solution. This study shows the effect of the stability of the DC voltages on the PMSM performances. The results obtained are full of promise to use the inverter in high voltage and great power applications as electrical traction.

REFERENCES

[1] D.Y. Lee, H.J. Noh, D.S. Hyun and I. Choy, '*An Improved MPPT Converter using Current Compensation Method for Small Scaled PV-Applications*', Eighteenth Annual IEEE, Applied Power Electronics Conference and Exposition, APEC'2003, Vol. 1, pp. 540 – 545, 9-13 February 2003.

[2] O. Gergaud, B. Multon and H. Ben Ahmed, '*Analysis and Experimental Validation of Various Photovoltaic System Models*', 7th International Electrimacs Congress, Montréal, pp. 1 – 6, August 2002.

[3] M. Hatti, '*Contrôleur Flou pour la Poursuite du Point de Puissance Maximum d'un Système Photovoltaïque*', Actes du Congrès Jeunes Chercheurs en Génie Electrique, JCGE'08, Lyon, 16 et 17 Décembre 2008.

[4] F. Belhachat, C. Larbes, L. Barazane et S. Kharzi, '*Commande Neuro-Floue d'un Hacheur MPPT*', 4th International Conference on Computer Integrated Manufacturing, CIP'2007.

[5] Y. Fu and B. Robyns, '*Digital Control of a PM Synchronous Actuator Drive System with a Good Power Factor*', Proceedings of the 13th IMACS'91, World Congress on Computation and Applied Mathematics, Dublin, Vol. 4, pp. 1538 – 1541, 22-26 July 1991.

[6] A. Brahmi, A. Abounada et M. Ramzi, '*Application de la Commande 'Perturb and Observe' pour l'Extraction de la Puissance Maximale des Cellules Photovoltaïques*' Revue des Energies Renouvelables CER'07 Oujda, pp. 121 – 124, 2007.

[7] M. Makhlouf, '*Etude et Optimisation d'un Modèle de Conversion d'Energie Photovoltaïque, Application au Pompage*', Mémoire de Magistère, Université Mentouri Constantine, 2006.

[8] E. Bueno, S. Cobreces, F.J. Rodriguez, F. Espinosa, M. Alonso and R. Alcazaz, '*Calculation of the DC-bus Capacitors of the Back-to-back NPC Converters*', EPE-PEMC 2006, 12th International Power Electronics and Motion Control, pp. 137 – 142, Portoroz, Slovenia, Aug. 30 - Sept. 1, 2006.